*Journal of Materials Chemistry A*

# Supporting Information

# High-Rate Capability and Long-Term Cycling of Self-Assembled Hierarchical $Fe_3O_4$/Carbon Hollow Spheres through Interfacial Control

Jing Huang, Songpu Cheng, Yuxi Chen,* Zhanglong Chen, Hao Luo, Xiaohong Xia, Hongbo Liu

College of Material Science and Engineering/Hunan Province Key Laboratory for Advanced Carbon Materials and Applied Technology, Hunan University, Changsha, 410082, China

** To whom correspondence should be addressed:*

*Yuxi Chen, Professor*

*Email: yxchen@hnu.edu.cn*

*Fax:+86-731-88823554*

*Tel: +86-731-88664018*

**1. Calculation of electrical conductivity:** 10 measurements of the electrical resistivity ρ (Ω cm) of each sample have been conducted, and the values are shown in the following table. The electrical conductivity σ (S $cm^{-1}$) is calculated based on the following equation,

$$\sigma = 1/\rho.$$

The reported σ of each sample is an average of 8 values except the largest and the lowest ones. The standard division of each sample is also given out.

| | 1st | 2nd | 3rd | 4th | 5th | 6th | 7th | 8th | 9th | 10th |
|---|---|---|---|---|---|---|---|---|---|---|
| H-F/CN | 10.01 | 19.97 | 10.06 | 10.26 | 10.37 | 10.22 | 9.77 | 9.91 | 10.01 | 10.02 |
| H-F/C | 226.3 | 199.8 | 209.7 | 216.5 | 207.4 | 136.7 | 260.2 | 201.4 | 209.5 | 211.4 |
| S-F/CN | 799.6 | 803.5 | 803.0 | 797.8 | 688.1 | 765.3 | 768.3 | 799.1 | 731.5 | 760.1 |
| S-F/C | 1993 | 1985 | 2030 | 2015 | 2006 | 1995 | 2065 | 2035 | 1998 | 1998 |

**2. Calculation of carbon content**: TG curves of the four samples (Figure 3g) depict that each curve exhibits two weight gain peaks located at ~300 °C and ~450 °C, respectively. It is reasonable to assume that the first weight gain peak (~300 °C) is associated with oxidation of the large-sized dense $Fe_3O_4$ layer, while the second peak is due to oxidation of the small-sized $Fe_3O_4$ layer inside of the sphere. Taking S-F/C as an example, the total weight loss is calculated to be the sum of "w1" and "w2". Thus the carbon contents of S-F/C, S-F/CN, H-F/C and H-F/CN are estimated to be ~15.7%, ~18.0%, ~28.3% and ~30.0%, respectively.

## Supporting figures

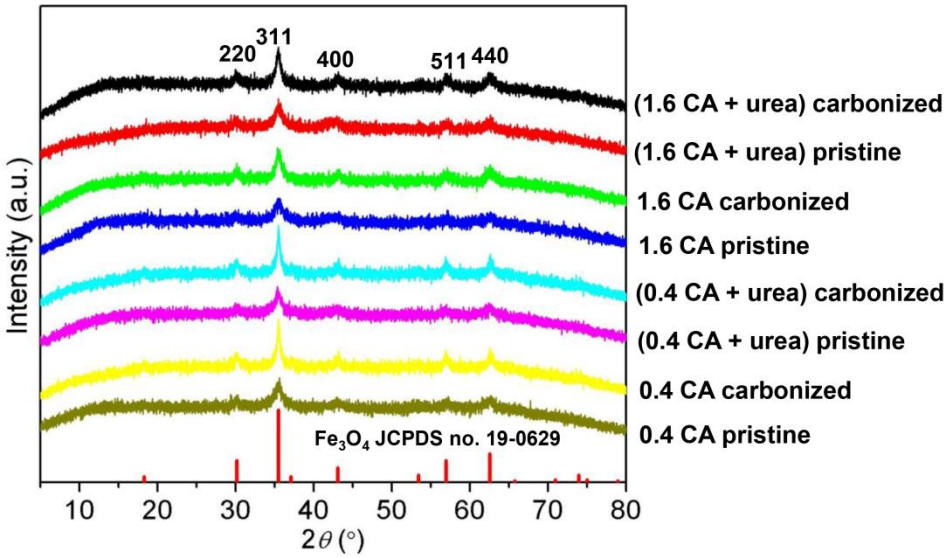


**Figure S1.** XRD patterns of the pristine products with CA contents of 0.4 g and 1.6 g (With or without urea addition) and the carbonized counterparts.

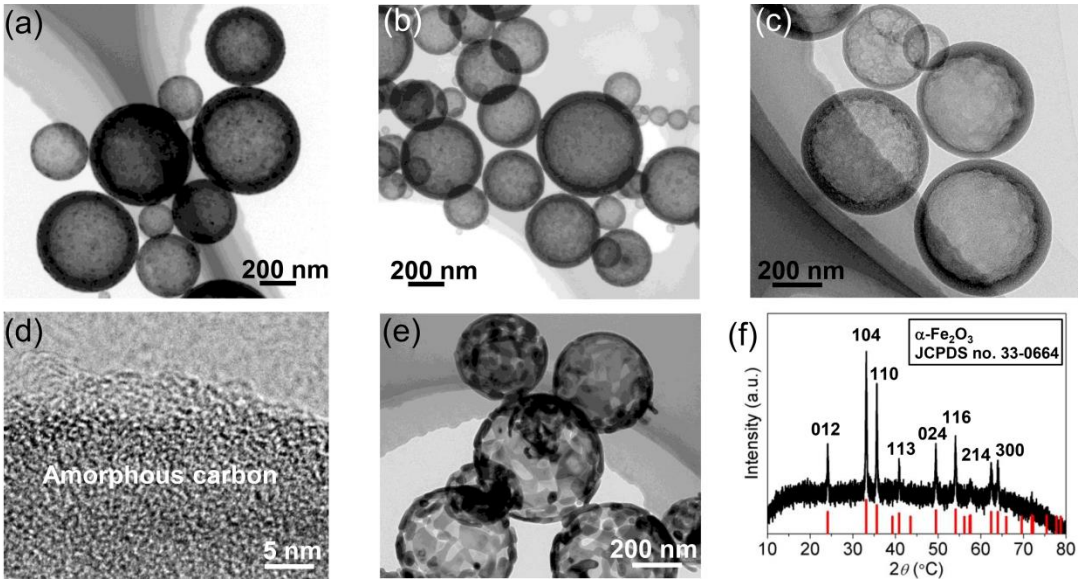


**Figure S2.** Microstructure of the new hollow-structured products originated from the pristine $Fe_3O_4$/carbon hollow spheres. (a) TEM image of the carbonized $Fe_3O_4$/carbon hollow spheres. (b) TEM image of the N-doped $Fe_3O_4$/carbon hollow spheres. (c) TEM image of the carbon hollow spheres. (d) High-resolution electron microscopy (HREM) image of the carbon hollow sphere. (e) TEM image of the porous α-$Fe_2O_3$ hollow cages. (f) XRD pattern of the porous α-$Fe_2O_3$ hollow cages. Standard diffraction positions of α-$Fe_2O_3$ are exhibited in the bottom.

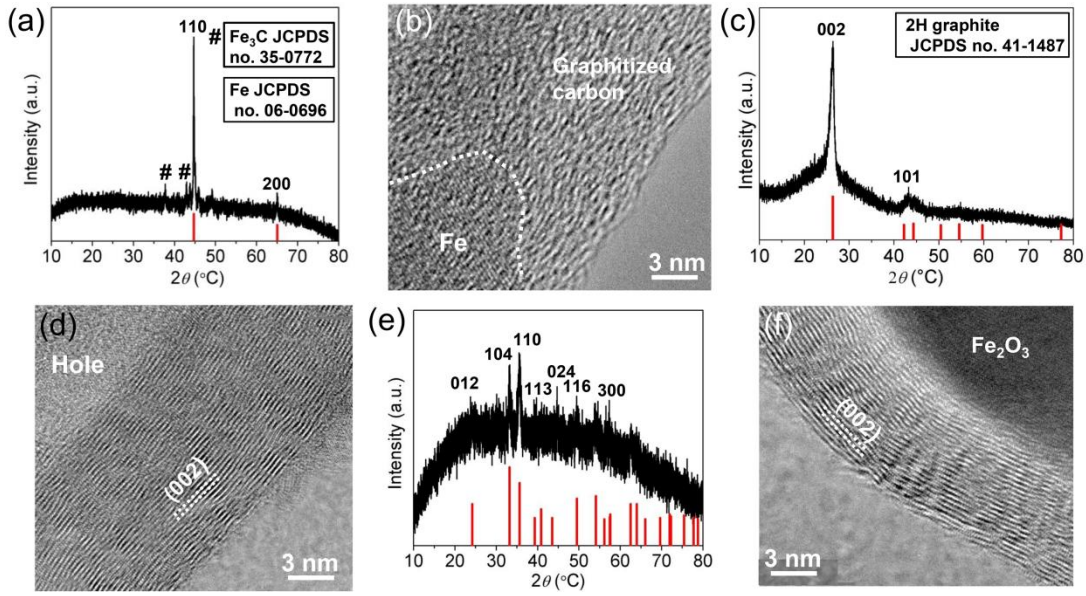


**Figure S3.** Microstructure of the graphitized carbon-based hollow structures originated from the pristine $Fe_3O_4$/carbon hollow spheres. (a) XRD pattern of the graphitized carbon/Fe hollow spheres. The standard diffraction positions of Fe are exhibited in the bottom. (b) HREM image of the graphitized carbon/Fe hollow sphere. The white dotted curve denotes boundary between Fe and graphitized carbon. (c) XRD pattern of the graphitized carbon hollow spheres. The standard diffraction positions of 2H-type graphite are depicted in the bottom. (d) HREM image of the graphitized carbon hollow sphere. (e) XRD pattern of the graphitized carbon/α-$Fe_2O_3$ hollow spheres. The standard diffraction positions of α-$Fe_2O_3$ are exhibited in the bottom. (f) HREM image of the graphitized carbon/α-$Fe_2O_3$ hollow sphere.

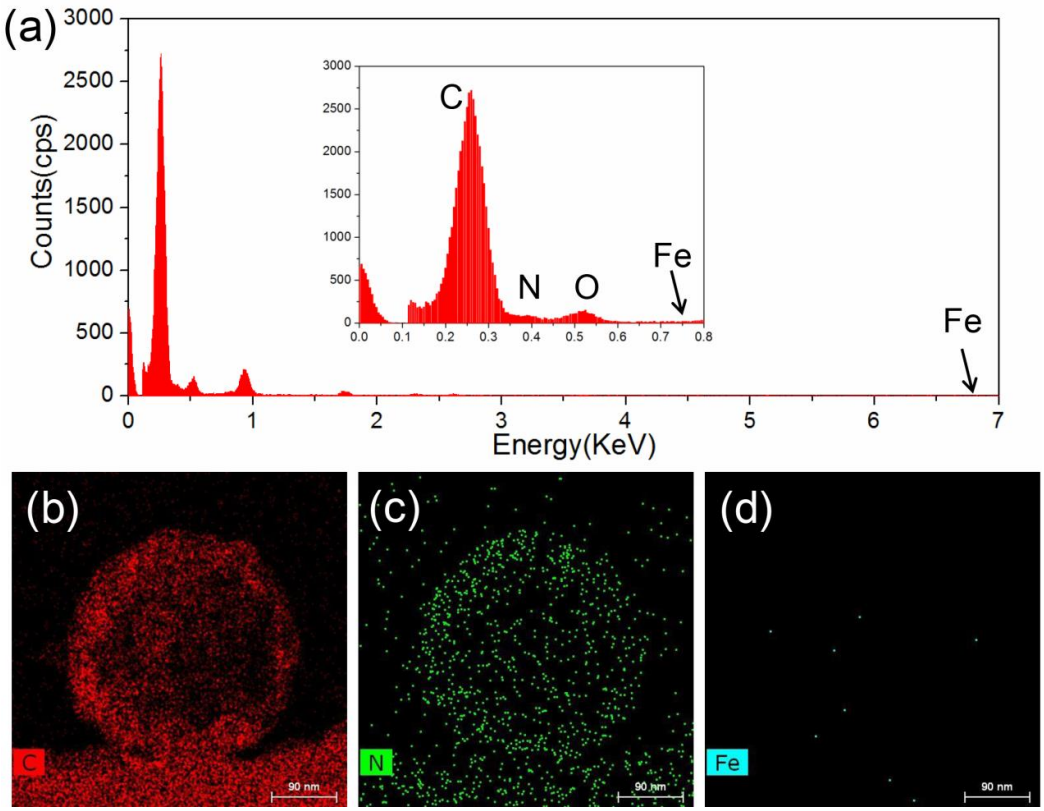


**Figure S4.** (a) EDS of the graphitized carbon hollow spheres. Inset is enlarge area of energy region of 0~0.8 K eV. Element mapping of (b) carbon, (c) nitrogen and (d) iron in the graphitized carbon hollow sphere.

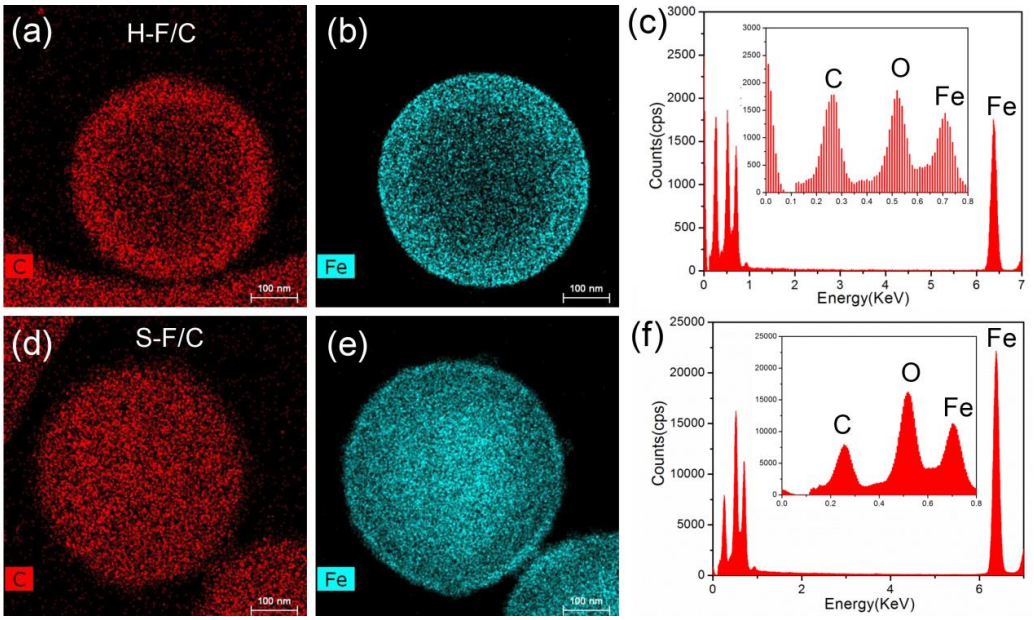


**Figure S5.** Element mapping of (a) carbon and (b) iron in H-F/C. (c) EDS of H-F/C. Element mapping of (d) carbon and (e) iron in S-F/C. (f) EDS of S-F/C.

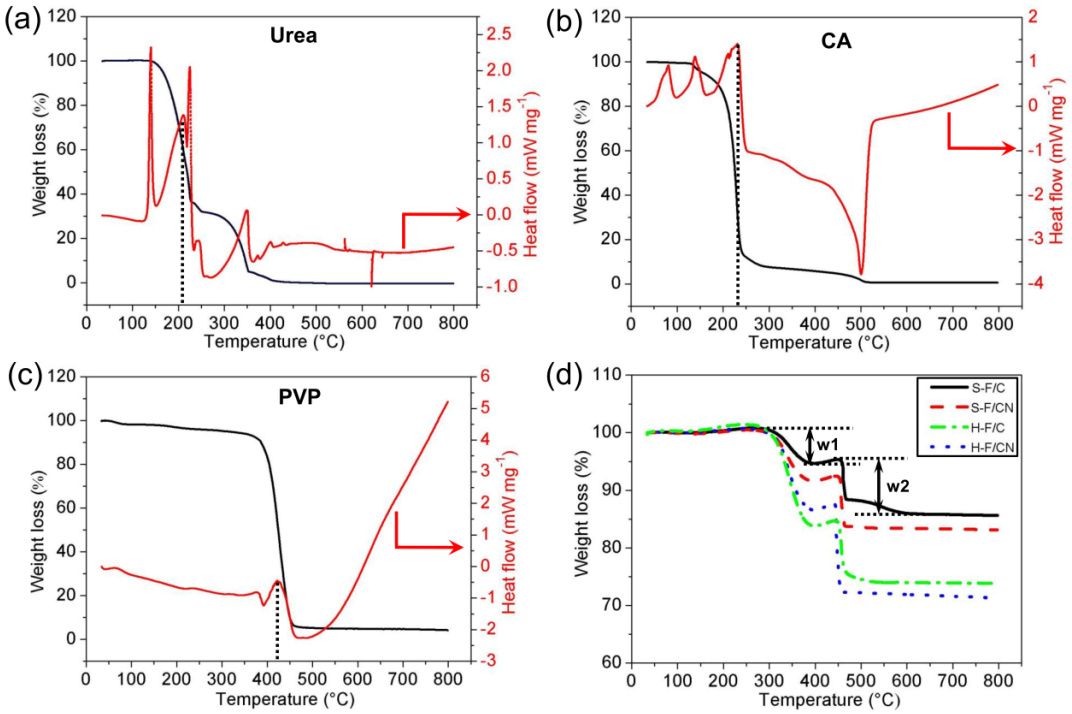


**Figure S6.** Thermal analysis of the starting materials and the four samples. (a) TG and differential thermal analysis (DTA) curves of urea. (b) TG and DTA curves of CA. (c) TG and DTA curves of PVP. The vertical dotted lines denote drastic pyrolysis temperatures. (d) TG curves of the four samples, “w1” and “w2” denote weight loss of each stage of S-F/C, respectively.

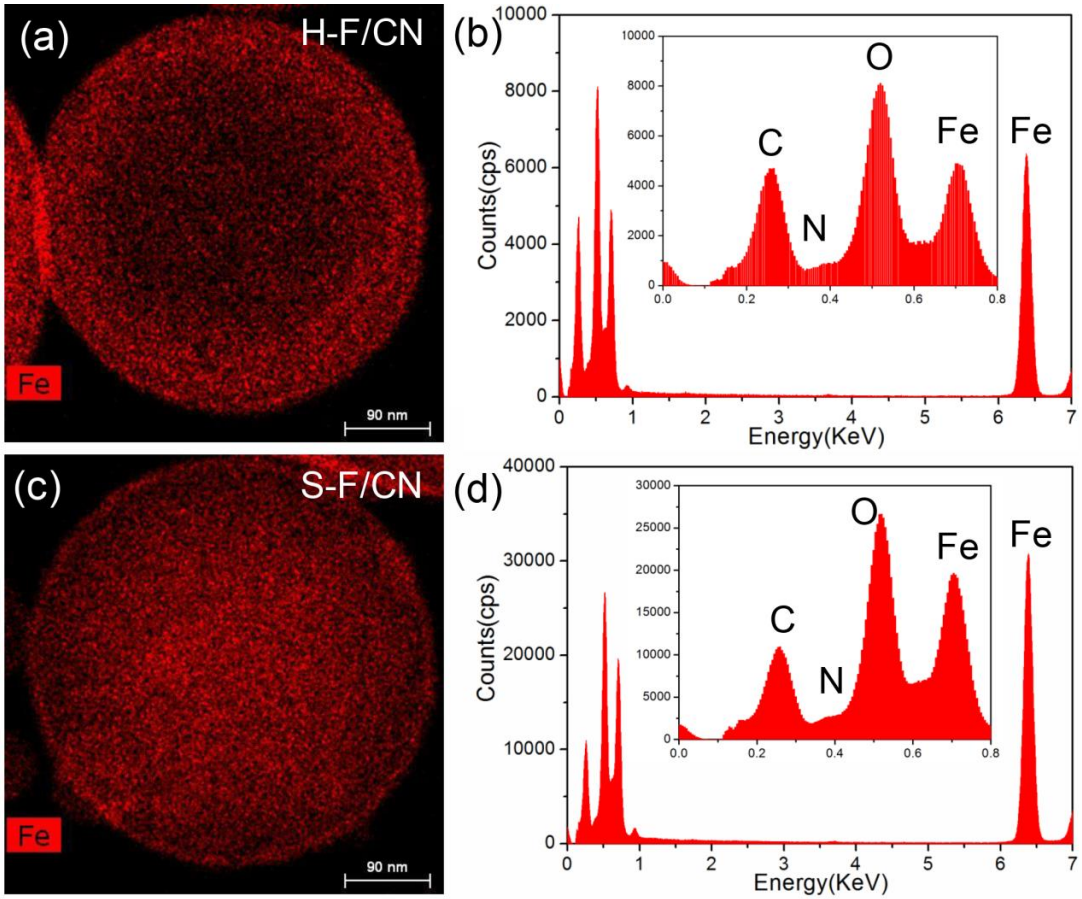


**Figure S7.** Element mapping of (a) iron in H-F/CN. (b) EDS of H-F/CN. Element mapping of (c) iron in S-F/CN. (d) EDS of S-F/CN.

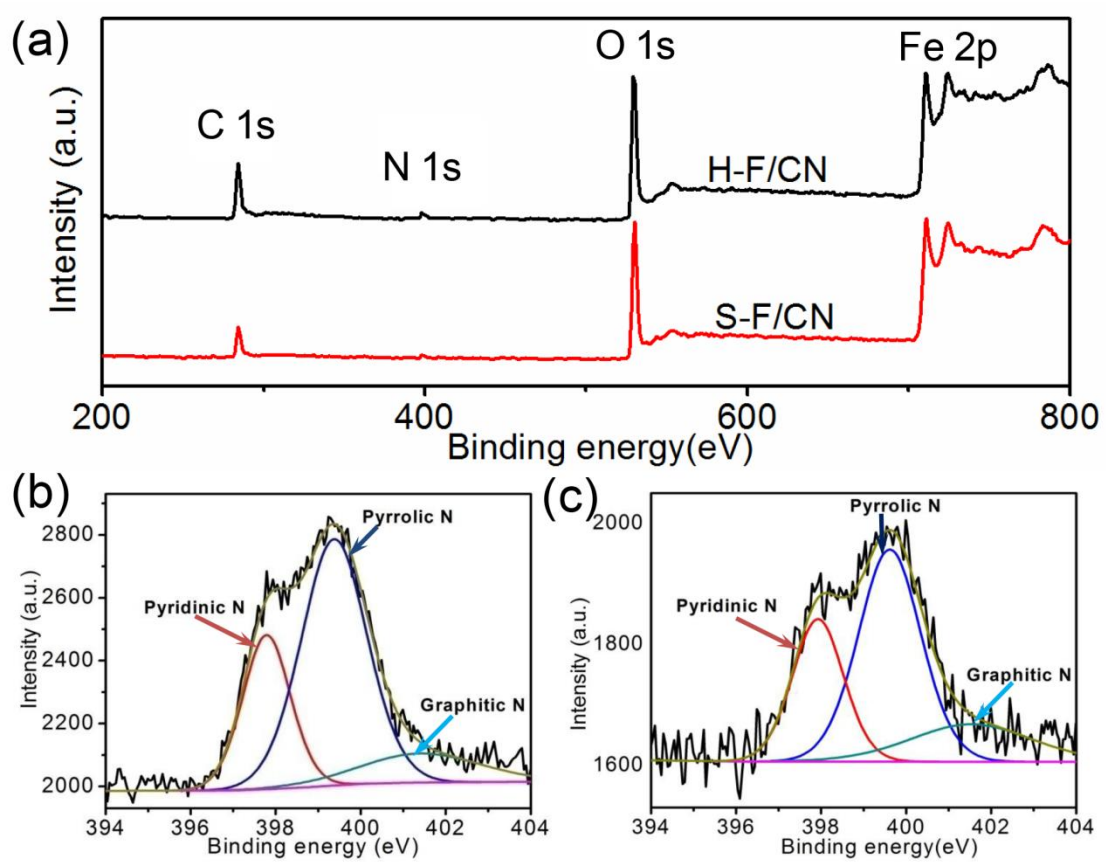


**Figure S8.** (a) XPS survey spectra of H-F/CN and S-F/CN, and high-resolution N1s peaks of (b) H-F/CN and (c) S-F/CN.

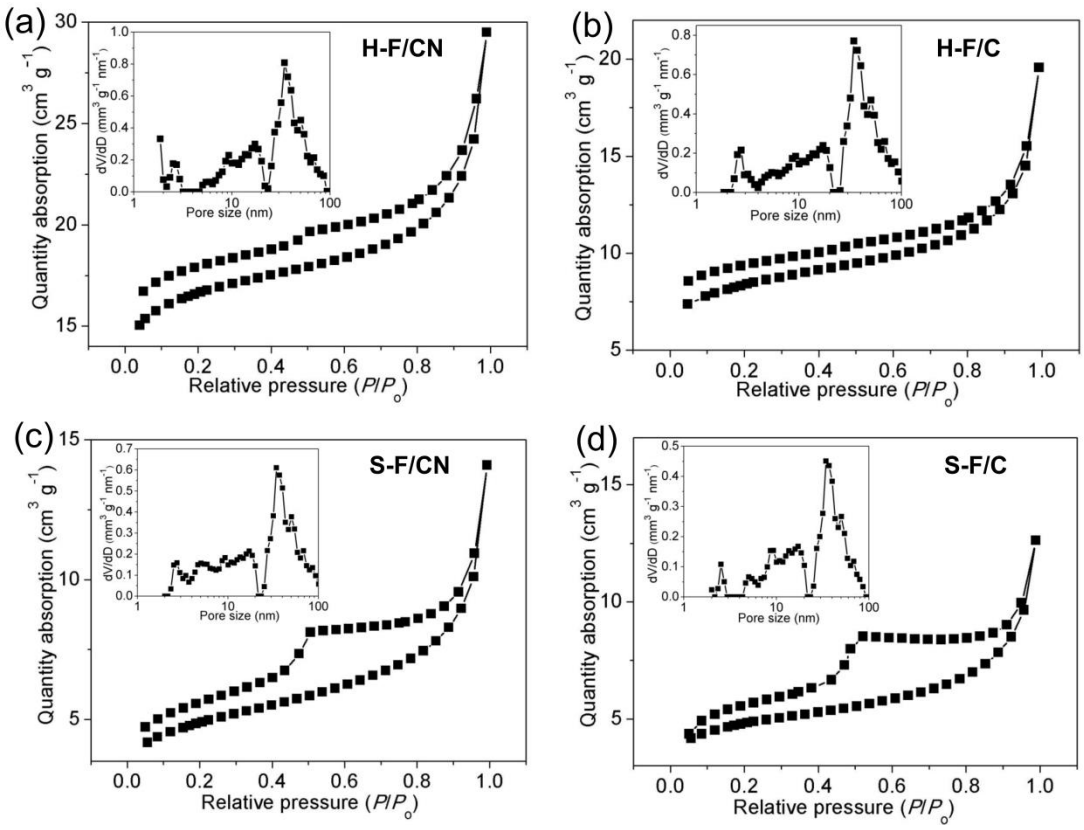


**Figure S9.** Nitrogen absorption/desorption isotherms and pore size distribution (Inset) of the four samples. **(**a) H-F/CN. (b) H-F/C. (c) S-F/CN. (d) S-F/C.

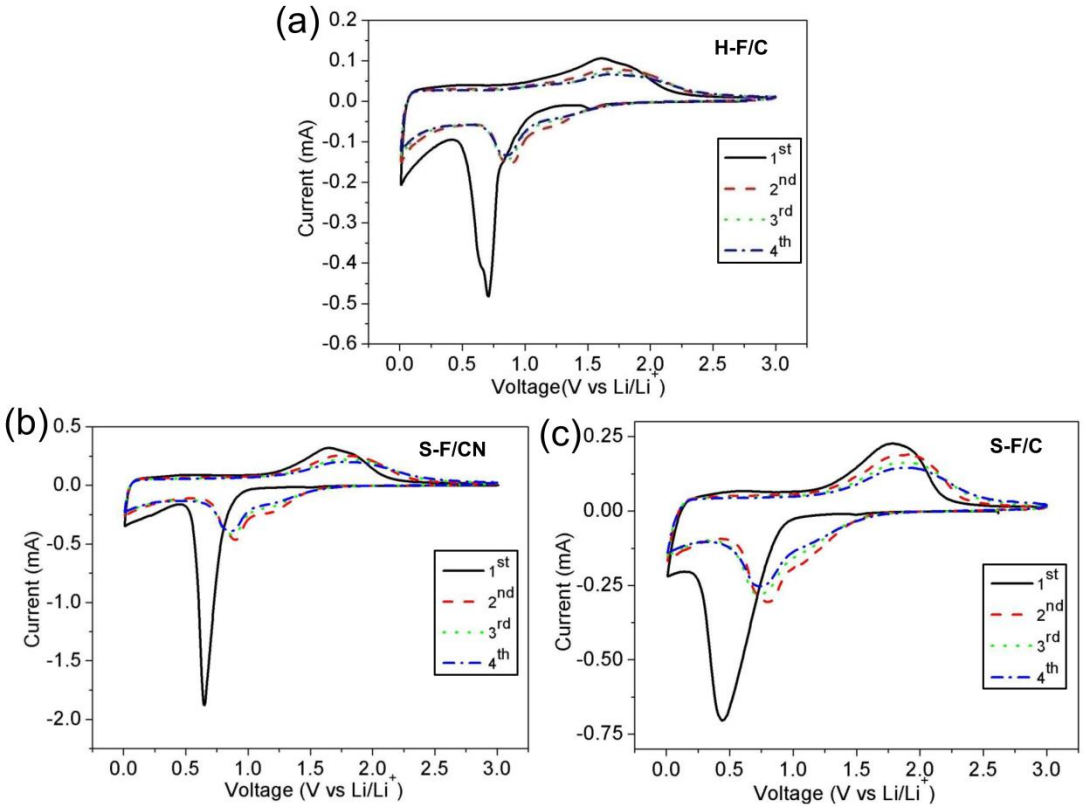


**Figure S10.** The initial four CV cycles of (a) H-F/C, (b) S-F/CN and (c) S-F/C.

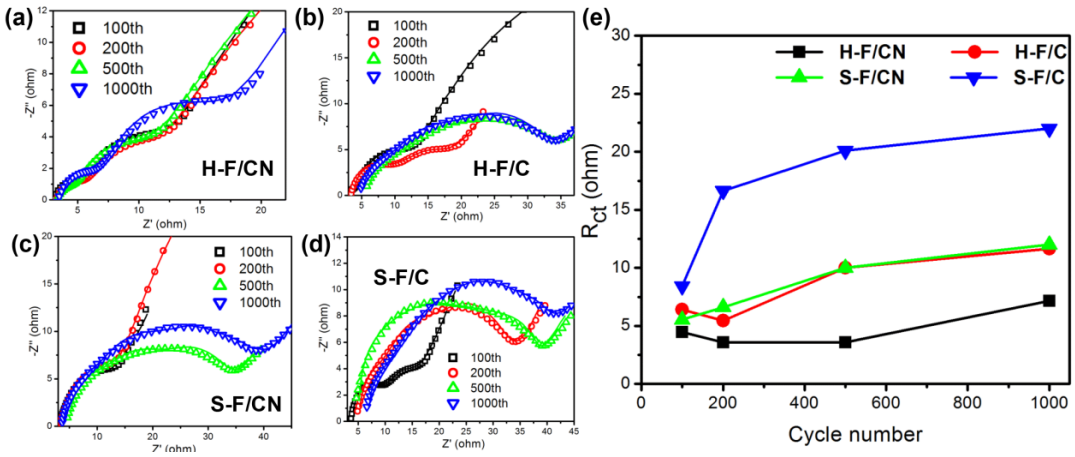


**Figure S11.** Nyquist plots of the four samples after different discharge/charge cycles at a current density of 10 A $g^{-1}$. (a) H-F/CN, (b) H-F/C, (c) S-F/CN and (d) S-F/C. The solid curves represent fitted data. (e) Plots of the charge transfer resistance $R_{ct}$s of the four samples after different discharge/charge cycles.

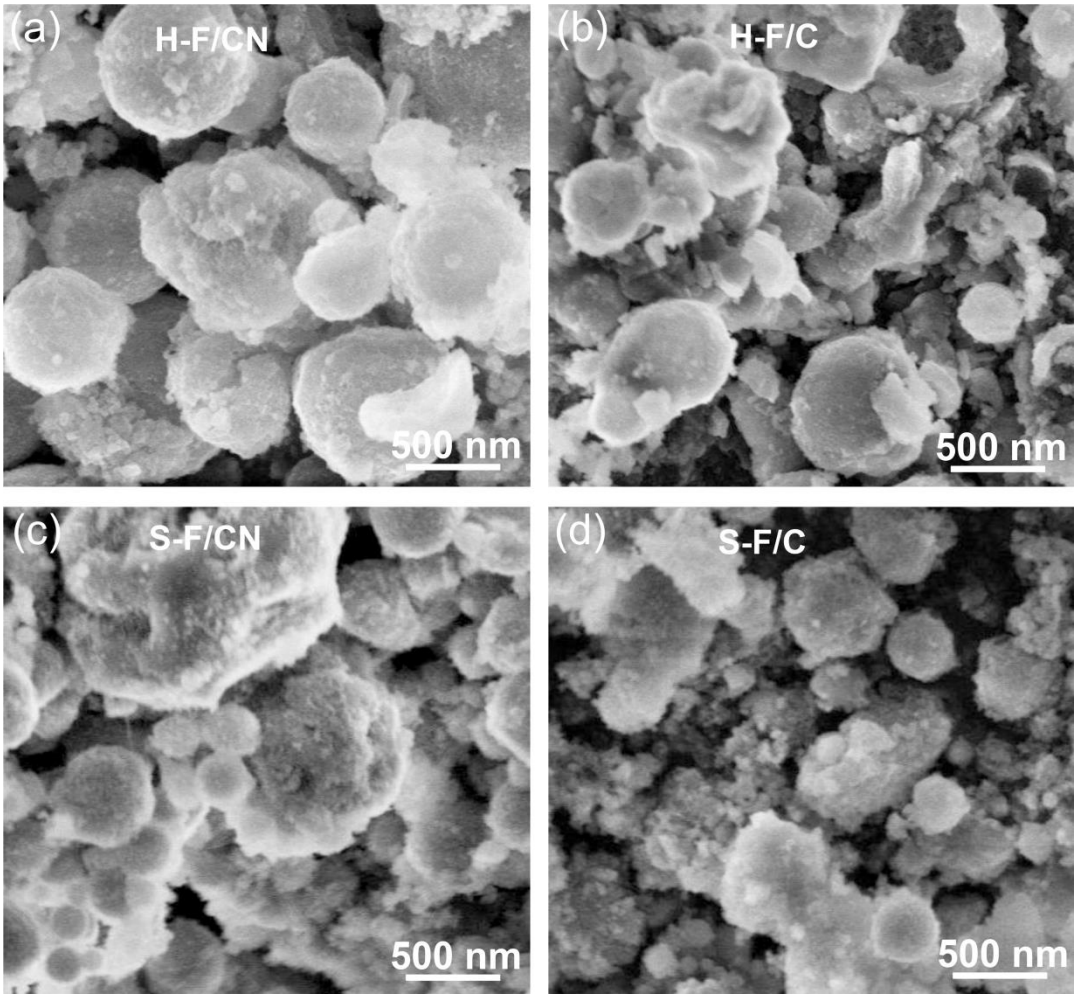


**Figure S12.** Scanning electron microscopy images of (a) H-F/CN, (b) H-F/C, (c) S-F/CN and (d) S-F/C after 1000 discharge/charge cycles at a current density of 10 A $g^{-1}$.

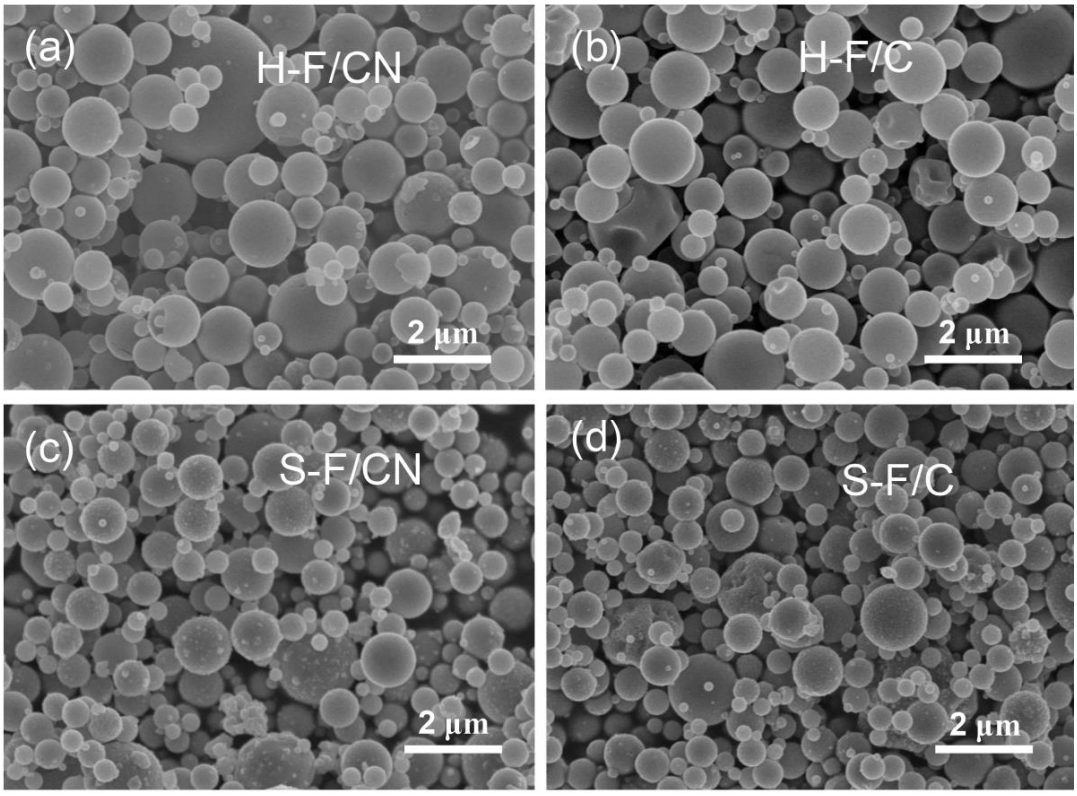


**Figure S13.** SEM images of (a) H-F/CN, (b) H-F/C, (c) S-F/CN and (d) S-F/C before discharge/charge cycling.